

Research Article

General Features of the Stellar Matter Equation of State From Microscopic Theory, New Maximum-Mass Constraints, and Causality

Francesca Sammarruca¹, Tomiwa Ajagbonna¹

¹. Physics Department, University of Idaho, United States

The profile of a neutron star probes a very large range of densities, from the density of iron up to several times the density of saturated nuclear matter, and thus no theory of hadrons can be considered reliable if extended to those regions. We emphasize the importance of taking contemporary *ab initio* theories of nuclear and neutron matter as the baseline for any extension method, which will unavoidably involve some degree of phenomenology. We discuss how microscopic theory, on the one end, with causality and maximum-mass constraints, on the other, set strong boundaries to the high-density equation of state. We present our latest neutron star predictions where we combine polytropic extensions and parametrizations guided by speed of sound considerations. The predictions we show include our baseline neutron star cooling curves.

Corresponding author: Francesca Sammarruca, fsammarr@uidaho.edu

I. Introduction

A fully microscopic equation of state (EoS) up to central densities of the most massive stars – potentially involving phase transitions and non-nucleonic degrees of freedom – is not within reach. Nevertheless, neutron stars are powerful natural laboratories for constraining theories of the EoS^{[1][2][3][4][5][6]}. One must be mindful of the theory's limitations and the best ways to extract and interpret information from observational constraints. Recently, detection of gravitational waves from merging of binary neutron star systems provided constraints on both their radius and tidal deformability.

Large Bayesian inference analyses have become popular as a tool to constrain the properties of neutron-rich matter. An example is Ref.^[7], where the authors sample 15,000 EoSs, together with observational constraints and heavy ion collision (HIC) data. These analyses are very important, but one must be careful about interpretation – relating HIC observables to parametrizations of the EoS is not a model-independent process. It is therefore not surprising that the authors of Ref.^[7] find that the HIC constraints tend to prefer stiffer EOSs than those favored by astrophysical observations, and, we add, stiffer than those generated by *ab initio* theory. The reasons can be found in the phenomenological QHD-inspired density functionals often used to relate HIC observables to the EoS parameters. This point will be discussed in sect. III.

When using sophisticated statistical techniques, it's important not to lose sight of basic physics arguments, such as the importance of a realistic description of few-body data. An extensive discussion on this point can be found in Ref.^[8].

In this paper, keeping a firm foot in the microscopic theory – that is, with no adjustments of nuclear forces in the medium – we wish to illustrate *general features* of the EoS in different density regions, based only on theory (for normal to moderately-above-normal densities), and a few robust constraints, such as causality and the most recent maximum-mass constraints^[9] (for high and superhigh densities).

The cooling properties of neutron stars, observationally accessible in terms of temperature (or luminosity) vs. age relations, are also an important tool to obtain a glimpse on the internal structure and composition of these exotic systems. Ages and thermal luminosities of neutron stars, inferred from observations, can be interpreted with the aid of the neutron star cooling theory to gain information on the properties of superdense matter in the interior of the star. We present our first results of cooling simulations, and compare with available observational estimates of thermally emitting isolated neutron stars (INS)^[10]. We recall that rapid cooling signals large proton fractions, which render the direct Urca (DU) process possible at lower densities as compared with softer models. Thus, rapid cooling signals a steep symmetry energy.

This paper is organized as follows. In sect. II, we review our theoretical ingredients, omitting details that have been published elsewhere. In sect. III, we discuss continuations of the EoS above the microscopic predictions. In sect. IV, we show preliminary predictions of cooling curves. A robust analysis of neutron star cooling, including superfluid gaps and more, will appear in a later work.

II. The equation of state at normal to moderately high density

A. Theoretical framework

The theoretical framework we use to obtain the *ab initio* part of the equation of state has been published in detail elsewhere^{[11][12][13]}, and thus we will not repeat a lengthy presentation here. We will, however, briefly recall the spirit of chiral effective field theory (EFT), on which our nuclear forces are based.

Given an energy scale, and degrees of freedom appropriate at that scale, an EFT comprises all interactions consistent with the symmetries that govern those degrees of freedom. For the nuclear problem, relevant degrees of freedom are pions (Goldstone bosons), nucleons, and $\Delta(1232)$ isobars. We use the delta-less chiral EFT. To begin with, one writes the most general Lagrangians describing all interactions between pions, nucleons, and pions with nucleons. Because pion interactions must vanish at zero momentum transfer and in the chiral limit, $m_\pi \rightarrow 0$, the corresponding Lagrangian is expanded in powers of derivatives or pion masses. From these Lagrangians, an infinite number of Feynman diagrams can be generated, which seems to make the theory unmanageable. The strategy is then to design a scheme for ordering the diagrams according to their importance – the essence of Chiral Perturbation Theory (ChPT). Nuclear potentials are defined by the irreducible types among these graphs. (By definition, an irreducible graph is a diagram that cannot be separated into two by cutting only nucleon lines.) These graphs are then analyzed in terms of powers of Q , with $Q = p/\Lambda_b$, where p is generic for a momentum, (nucleon three-momentum or pion four-momentum), or the pion mass, and $\Lambda_b \sim m_\rho \sim 0.7$ GeV is the breakdown scale^[14]. Determining the power ν has become known as power counting. For a recent review of nuclear forces based on chiral Effective Field Theory (EFT) and their applications in nuclear and neutron matter, the reader is referred to Ref.^[15].

B. Chiral orders and three-nucleon forces: unresolved issues

While the predictions at N²LO are fully *ab initio*, a warning is in place for current N³LO calculations. As pointed out in Ref.^[16], there is a problem with the regularized 3NF at N³LO (and higher orders) in all present nuclear structure calculations. The N³LO 3NFs currently in use are regularized by a multiplicative regulator applied to the 3NF expressions derived from dimensional regularization. This approach leads to violation of chiral symmetry at N³LO and destroys the consistency between two-

and three-nucleon forces^{[16][17]}. Consequently, none of the current calculations that include 3NFs at N³LO (and beyond) can be considered truly *ab initio*. An appropriate symmetry-preserving regulator^[16] should be applied to the 3NF at N³LO from Refs.^{[18][19]}. At the present time, reliable predictions exist only at N²LO, NLO, and LO. However, for the few fully *ab initio* calculations, the precision at N²LO is unsatisfactory. A first step towards deriving consistently regularized nuclear interactions in chiral EFT, has been proposed in Refs.^{[20][21]}. It requires the cutoff to be introduced already at the level of the effective Lagrangian. A path integral approach^[20] can then be applied to the regularized chiral Lagrangian to derive nuclear forces through the standard power counting of chiral EFT.

Throughout the paper, we will show results at the (fully consistent) third order (N²LO), and at the highest order which we have considered (fourth order, or N³LO). In Figure 1, we show the pressure as a function of density in β -stable matter at N²LO (red) and at N³LO (blue), with the respective truncation errors. In both cases, the predictions are based on the high-quality *NN* potential of Ref.^[22] and include all 3NFs required at that order. For details on how our EoS are built, see, for instance, Refs.^{[11][23]}.

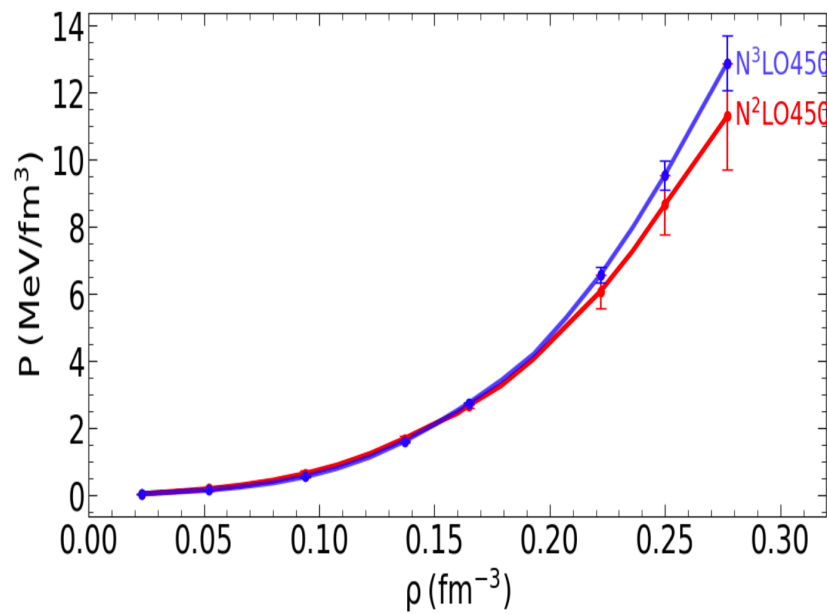


Figure 1. Pressure as a function of density in β -stable matter at N²LO (red) and at N³LO (blue), with the respective truncation errors. In both cases, the predictions are based on the high-quality *NN* potential of Ref. ^[22] and include all 3NFs required at the respective order.

III. The equation of state at high density

It is important to emphasize that high-density EoS continuations are not meant to be a replacement for microscopic theories which, at this time, are not feasible in those regimes. Nevertheless, causality and maximum-mass constraints do pose considerable restrictions on the general features of the high-density EoS.

Up to this point, we have used piecewise polytropes, which have the form:

$$P(\rho) = \alpha \left(\frac{\rho}{\rho_0} \right)^\Gamma, \quad (1)$$

where α and Γ are fitted to the boundary conditions, and ρ_0 is the density of saturated nuclear matter. We accepted polytropes which can support a maximum mass of at least $2.01 M_\odot$, to be consistent with the lower limit of the $(2.08 \pm 0.07) M_\odot$ observation reported in Ref. [6] for the J0740+6620 pulsar, along with a radius estimate of (12.35 ± 0.75) km. Figure 2 displays results of the procedure we used in the recent past. The $M(R)$ relations are obtained with piecewise combinations of two polytropes with different adiabatic index. Equations of state that cannot support a maximum mass of at least $2.01 M_\odot$ (see above), are discarded, and solutions are cut at the central density where causality is violated [23]. The initial range we considered for the adiabatic index, Γ , was approximately between 2.5 and 4.0, based on guidance from the literature, such as Ref. [24], where most of the EoS available from theory or phenomenology were fitted with polytropes.

Currently, the maximum-mass constraint must account for the record-setting PSR J0952-0607, the heaviest well-measured neutron star found to date, at $2.35 \pm 0.17 M_\odot$ [9]. We then explored different piecewise parametrizations of the high-density EoS that preserve causality, while supporting masses at least as high as $2.2 M_\odot$. We emphasize that *ab initio* predictions and most of the terrestrial constraints point to a soft symmetry energy at normal density, while the maximum mass constraint has moved to larger values. These considerations provide important guidance when building the phenomenological part of the EoS.

While checking different polytropic combinations, we made the observation that the “best” combination (with regard to preserving causality while satisfying maximum-mass constraints) consists of a relatively stiff polytrope attached to the microscopic piece of the EoS, followed by a second, softer polytrope. Although polytropic extension is a very general and popular method, alternative parametrizations of the high-density EoS offer desirable features [25][26], such as those in

terms of the speed of sound. In Figure 3, the colorful curves are from selected EoS that generate maximum masses of about 2.1 to 2.2 solar masses and are consistent with causality. Table 1 provides more information about these cases. The black curve is obtained with a single parametrization in terms of the speed of sound, constructed as in Refs. [25][26]. Assigning $i = 0$ to values at threshold (the density at which the EoS parametrization has to be attached to the previous piece), we write

$$\rho_i = \rho_{i-1} + \Delta\rho, \quad (2)$$

$$\epsilon_i = \epsilon_{i-1} + \Delta\epsilon, \quad (3)$$

and

$$\Delta\epsilon = \Delta\rho \frac{\epsilon_{i-1} + P_{i-1}}{\rho_{i-1}}. \quad (4)$$

The speed of sound is parametrized as

$$\left(\frac{v_s}{c}\right)_i^2 = 1 - c_1 \exp\left[-\frac{(\rho_i - c_2)^2}{w^2}\right], \quad (5)$$

where the constants c_1 and c_2 are determined from continuity of the speed of sound and its derivative at the threshold density. Finally, the pressure above the threshold is

$$P_i = \left(\frac{v_s}{c}\right)_{i-1}^2 \Delta\epsilon + P_{i-1}, \quad (6)$$

where we have used the basic relation between pressure and energy density. This EoS continuation is manifestly causal at any density and reaches a maximum mass of $2.07 M_\odot$.

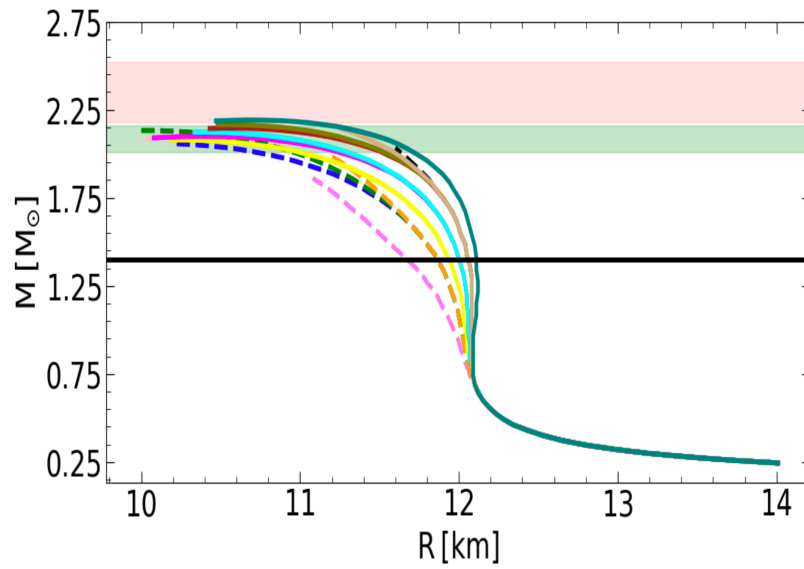


Figure 2. $M(R)$ relations obtained with piecewise polytropes^[23]. Equations of state that cannot support a maximum mass of at least $2.01 M_{\odot}$ (see text) are discarded. Curves are cut at the central density where causality is violated. The black horizontal line marks the mass of the canonical neutron star, for reference. The green and pink shaded areas are constraints from J0740 + 6620^[27] and J0952 - 0.607^[9], respectively.

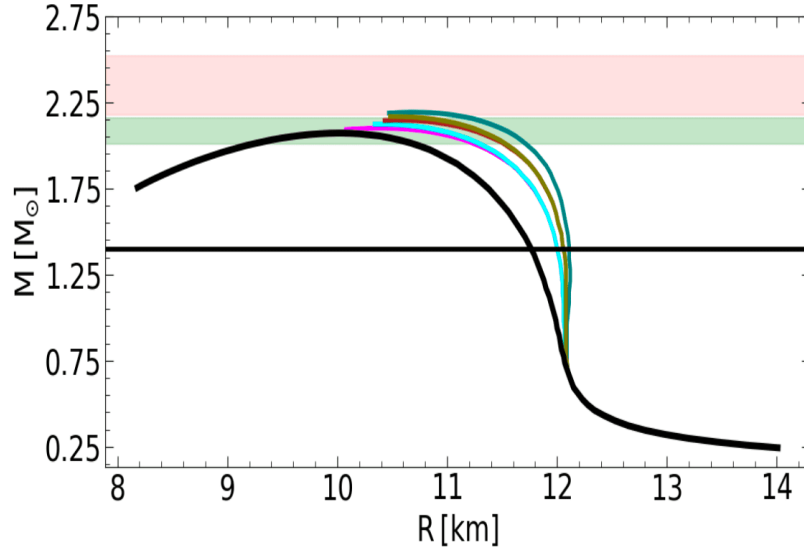


Figure 3. Several $M(R)$ relations. The curves in color are obtained from a sequence of two polytropes with adiabatic indices given in Table 1. The black curve is obtained with a single parametrization in terms of the speed of sound, as in Eq. (6).

curve color	Γ_1	Γ_2	M_{\max}/M_{\odot}	$R_{1.4}$ (km)
magenta	3.1	2.7	2.10	12.00
cyan	3.1	2.8	2.12	12.00
brown	3.2	2.7	2.15	12.06
olive	3.2	2.8	2.17	12.06
green	3.3	2.7	2.19	12.11

Table 1. Description of the $M(R)$ relations in Figure 3.

We find that a better solution is to combine a relatively steep (on the scale of Table 1) polytrope followed by a parametrization obtained from Eqs. (5-6), which will maintain causality by construction. The matching densities are $\rho_1 = 0.277\text{fm}^{-3}$ and $\rho_2 = 0.563\text{fm}^{-3}$. The rationale for the first matching density is as follows. The *neutron* Fermi momentum in neutron matter, k_F^n , at ρ_1 is

equal to 0.202 fm^{-1} . Of course, this is larger than the momentum in beta-stable matter at the same density due to the presence of a proton fraction,

$$k_F^{snm} < k_F^\beta < k_F^n, \quad (7)$$

where k_F^{snm} and k_F^β are the Fermi momentum in symmetric nuclear matter and in beta-stable matter, respectively. The average momentum of a neutron Fermi gas is given by:

$$P_{av} = \sqrt{\frac{3}{5}} k_F^n, \quad (8)$$

which we take as the typical momentum of the system, p , in defining the chiral expansion parameter, $Q = \frac{p}{\Lambda_b}$, where Λ_b is the breakdown scale, approximately 600 MeV. We obtain $Q = 51\%$, which is well below 1, and actually a pessimistic estimate, see Eq. (7). For these reasons, we are comfortable applying the EFT up to this density. The density ρ_2 is about two units of ρ_0 from the first matching point.

The resulting $M(R)$ curves are shown in Figure 4 for both N³LO (blue) and N²LO (red). For the dashed curves, the first extension is done with a polytrope with $\Gamma = 3.3$, followed by pressure values given by Eq. (6) with the speed of sound (SoS) as in Eq. (5). The solid curves (same color convention) have been obtained with $\Gamma = 3.8$, a value beyond which the EoS begins to violate causality, see also Figure 5. Table 2 displays the maximum mass, its radius, the central density, and the radius of the canonical mass neutron star, for the curves in Figure 4. We recall that the radius of a $1.4 M_\odot$ is sensitive to the pressure at normal densities and thus it can pose constraints on microscopic theories of the EoS at those densities where such theories are applicable

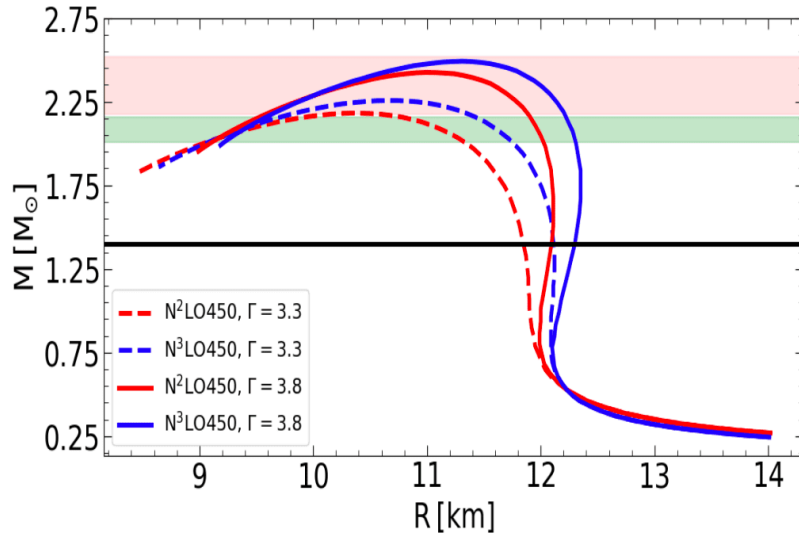


Figure 4. $M(R)$ curves at fourth order (N^3LO , blue) and at third order (N^2LO , red) of ChPT. Dashed curves: the first extension is done using a polytrope with $\Gamma = 3.3$, followed by pressure values given by Eq. (6) together with Eq. (5); Solid curves: obtained with $\Gamma = 3.8$, a value beyond which the EoS begins to violate causality.

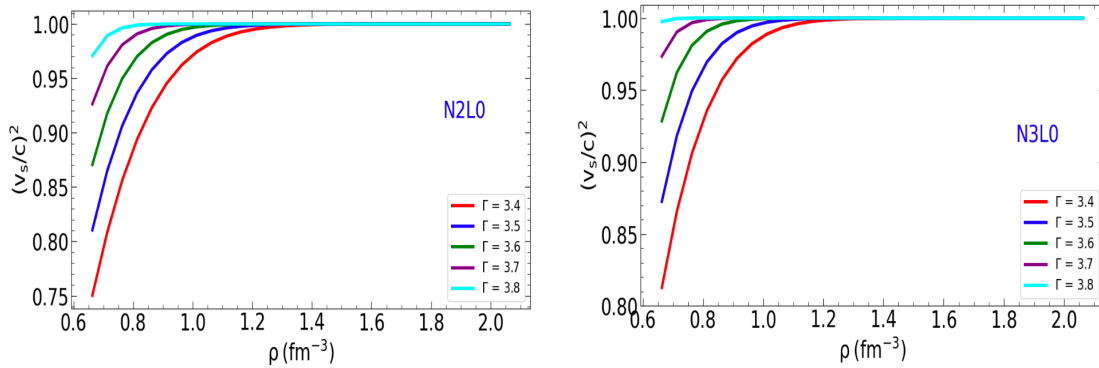


Figure 5. Speed of sound, in units of the speed of light, at N^2LO (left) and at N^3LO (right).

The speed of sound as a function of density is shown in Figure 5. In each case, a single polytrope with the shown value of Γ is followed by the SoS-guided EoS. Thus, a polytrope that bridges the chiral EFT predictions with a causality-maintaining parametrization, has a limited range of powers. We underline that this scenario is inherently related to the softness of the chiral predictions. In other

words, the nature of the predictions at normal density have a far-reaching impact, which extends to densities up to a few times normal density.

Γ	chiral order	M_{max}/M_{\odot}	$R_{M_{max}}(km)$	$\rho_c(fm^{-3})$	$R_{1.4}(km)$
3.3	N ² LO	2.18	10.34	1.12	11.84
	N ³ LO	2.26	10.70	1.01	12.11
3.8	N ² LO	2.42	10.99	0.94	12.09
	N ³ LO	2.49	11.31	0.88	12.30

Table 2. Some neutron star properties corresponding to the red and the blue M(R) relations shown in Figure 4.

Of course, what we have presented is not the only option for building EoS that are consistent with current astronomical observations. We maintain, though, that an EoS must be “bounded from below” by free-space few-nucleon data (which, in turn, have a strong impact on the symmetry energy and the pressure in neutron-rich matter at normal densities). Typical examples of the other end of the spectrum are phenomenological EoS, such as those from RMF models. With no constraints from microscopic few-nucleon forces, new parametrizations can be constructed using different nonlinear, self- and inter-couplings among meson and nucleon Dirac fields^[28]. Isovector mesons carry isospin dependence, with the main contribution to the symmetry energy coming from the pion^[29]. In the RMF (pionless) framework, the interplay between the isovector ρ and δ is described as the equivalent, in the isovector channel, of the $\sigma - \omega$ interplay in the isoscalar channel. This approach, and the resulting couplings, have little to do with free-space NN interactions^[29]. Not surprisingly, parametrizations can be found to cover a huge range of EoS “stiffness,” most recently incorporating CREX and/or PREX-II constraints^[28]. Findings from RMF models concerning, especially, isovector quantities, such as the symmetry energy, must be interpreted with caution.

IV. Cooling of neutron stars

A. General considerations

To create context, we review here some basic facts about INS cooling.

Accurate modelling of neutron star cooling with account of all possible effects is a complex problem. Cooling can be affected, for instance, by the presence of free hyperons or deconfined quarks (see Ref. [30] and references therein), and pion or kaon condensation (see Ref. [31] and references therein).

The internal structure of the neutron star can be taken, to a good approximation, to be spherically symmetric, except for fast rotating INS or strong magnetic fields. It is also reasonable to expect that the temperature distribution is spherically symmetric at sufficiently high densities. Under these assumptions, the mechanical structure and temperature distribution are determined by a set of differential equations [32] which involve only one spatial coordinate, the radial coordinate r .

Neutron stars cool down mainly via neutrino emission from their cores and photon emission from their atmospheres. They are relativistic objects, and thus one needs to be careful about the coordinate system. The local temperature at some distant r from the center is related to the temperature, T^∞ , measured by a distant observer, via the gravitational redshift between the coordinate systems:

$$T^\infty = e^{\phi(r)} T(r), \quad (9)$$

where ϕ is the metric function.

The outermost layer of a neutron star is the *atmosphere*, consisting of gas elements which emit thermal photons that can be observed on the earth. Surface luminosity and temperature can be inferred by fitting this photon flux, and is a major source of cooling for older neutron stars. Below the atmosphere, there is a thin region called *envelope*, whose chemical composition is uncertain.

Although the distribution of the surface temperature over the surface can be non-uniform, it is customary to approximate the surface photon emission as the blackbody radiation from the entire surface. To that end, one introduces the overall surface effective temperature of the star, $T_{s,\text{eff}}$, related to the photon luminosity, L_γ , by

$$L_\gamma = 4\pi\sigma_{\text{SB}}R^2T_{s,\text{eff}}^4, \quad (10)$$

where σ_{SB} is the Stefan-Boltzmann constant. The quantities in the above equation refer to a local reference frame at the neutron-star surface. Those detected by a distant observer are redshifted,

$$L_\gamma^\infty = L_\gamma(1 - r_g/R) = 4\pi\sigma_{\text{SB}}R_\infty^2(T_{s,\text{eff}}^\infty)^4, \quad (11)$$

$$T_{s,\text{eff}}^\infty = T_{s,\text{eff}}\sqrt{1 - r_g/R}, \quad R_\infty = R/\sqrt{1 - r_g/R}, \quad (12)$$

where r_g is the Schwarzschild radius, $r_g = \frac{2GM}{c^2}$.

Either surface temperatures or photon luminosities can be used to compare neutron-star observations with the cooling theory. Both can be obtained with spectral analysis, but accurate determination is usually a challenge. One of the problems with obtaining accurate data suitable for testing the theory of cooling is that the vast majority of neutron stars, including INS, emit intense radiation of non-thermal origin. Neutron star binary systems are usually surrounded by an accretion disk, whose emission is orders of magnitude more powerful than the thermal emission from the neutron star surface^[33]. Non-thermal emission of INS can also be produced by other processes, and thus a careful analysis is required to extract the thermal component of the observed spectrum. Another problem is that obtaining the ages of neutron stars from observation is difficult, and thus ages are only estimates. Neutron stars that are estimated to be old have lost their initial heat, and therefore their thermal luminosity is very low, and could have been produced by reheating^{[34][35]}.

In summary, the “standard” cooling theory, which neglects reheating, can only be tested against observations of a small fraction of INS, using estimated ages.

B. Baseline results

In this section, we perform cooling simulations employing the two EoS used to generate the red and blue $M(R)$ dashed curves in Figure 4. Our beta-stable EoS include protons, electrons, and muons.

From Figs. 6 and 7, one can see the mass dependence of the effective temperature and the closely related luminosity, see Eq. (10). The more massive INS correspond to faster cooling, suggesting that enhanced neutrino emission due to DU reactions operates in those stars, where the proton fraction in the interior reaches values sufficient to enable the process. Pairing, not included here, could suppress DU processes. The data are from Ref. ^[36].

The difference between Figure 6 and Figure 8 is the model for the envelope. In Figure 6, the envelope contains light elements up to densities where they can still be present, and heavier elements, including iron, at the higher densities^[37]. In Figure 8, older iron models for the envelope^[38] are employed. We see that the chemical composition of the envelope has a significant impact on the cooling curves, especially for low to medium mass neutron stars. The envelope acts as a thermal

insulator between the surface and the hot interior, thus relating interior temperature to the star's effective surface temperature. There is a large temperature gradient between the top and bottom layers of the envelope, determined by the amount of light elements such as Hydrogen or Helium. Therefore, the composition of the envelope impacts the photon cooling of the envelope.

Some investigations^[33] have concluded that an EoS allowing DU cooling for a wide enough mass range of neutron stars, combined with some quenching by the proton 1S_0 BCS gap, agrees best with the cooling data, while the neutron pairing gap in the triplet P -wave seems to generate overly rapid cooling. Others^[39] find that pairing in the triplet P -states prevail in neutron matter, but essentially disappear if the spin-orbit interaction is turned off. Overall, the contribution from pairing is quite sensitive to the characteristics of the model.

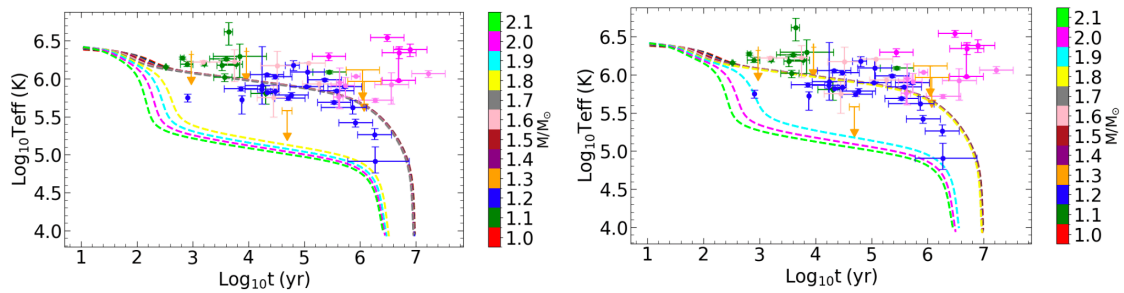


Figure 6. Effective temperature as a function of time, for different masses (colors). Left: N²LO; Right: N³LO. The envelope from Ref. ^[37] is applied.

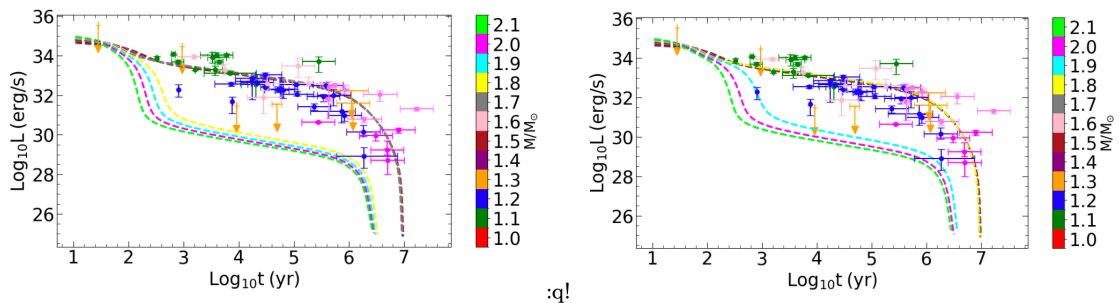


Figure 7. Photon luminosity as a function of time, for different masses (colors). Left: N²LO; Right: N³LO. All conditions as in Figure 6.

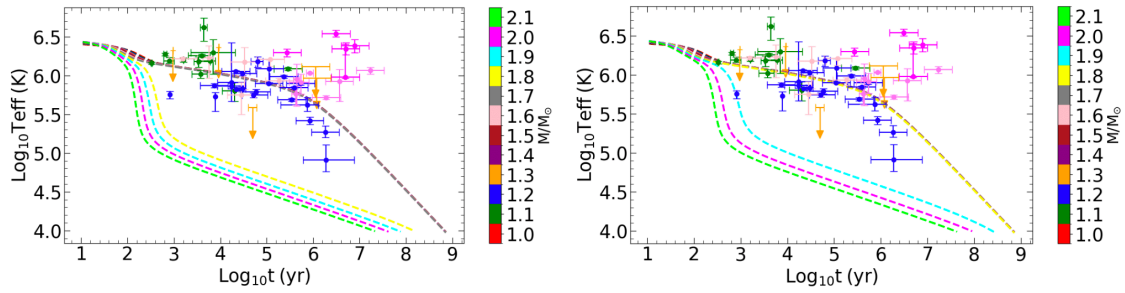


Figure 8. As in Figure 6, but with envelope model from Ref. [38].

V. Conclusions and work in progress

The intrinsic and strong relation between the EoS and the maximum mass of a neutron star sequence is a remarkable feature. In fact, knowledge of one is essential to access the other. In our observations, the maximum-mass constraint moving to higher values, together with the causality requirement at any central density, poses significant restrictions on the high-density EoS. The softness of the microscopic predictions at normal density brings up the need for a (first) steeper extension. A scenario such as the one we have described, where the first part of a piecewise extension needs to become stiffer in order to support current maximum mass constraints, while the next piece must soften to maintain causality, would suggest that phase transitions and/or exotic species begin to appear only at the highest densities, where the composition of a neutron star is very unlikely to become known in the foreseeable future.

We reiterate that a microscopic theory of the nuclear many-body problem must start from quantitative descriptions of few-nucleon interactions. Those constraints have implications at normal density and well beyond it.

We also took the opportunity to display cooling curves as the foundation of a forthcoming comprehensive analysis, including gaps and medium effects. The sensitivity of gaps to medium effects on the input interaction can be dramatic, in both S and P states. Short-range correlations (SRC) are the most model-dependent part of a potential, and may play a significant role for the gap^[40]. Typically, one would expect SRC to reduce the gap by introducing more high-momentum components and thus removing strength around the Fermi level and depleting the gap^[40]. As the $1S0$ interaction turns repulsive with increasing density, the gap disappears and one opens in the triplet channel, at a

Fermi momentum close to 1.0 fm^{-1} . Attractive noncentral interactions are essential for $1S0$ superfluidity. The scenario is more complex for the triplet coupled channel ($3P2 - {}^3F2$) in part because of the higher densities involved. Also, the $3P2$ gap is more sensitive to the pairing interaction than the S-wave gap, because it is small compared to the Fermi energy.

Considerable work has been done in recent years on neutron matter gaps, sometimes with contradictory results. In Ref. [41], where the predictions are based on the Argonne V18 potential, a huge enhancement of the gap results from the inclusion of a 3NF. At the higher orders of chiral EFT and with semilocal chiral potentials with varying cutoff, a maximum gap of 0.4 MeV was predicted around $1.7\text{-}1.9 \text{ fm}^{-1}$ [42], and found to be very sensitive to the interaction, the chiral order, and the cutoff. In Ref. [43], the gap equation for the triplet P channel in neutron matter was solved using the AV18 NN potential and two alternative versions of the UIX 3NF. It seems that the two parameterizations of the Urbana 3NF give conflicting answers to the question of whether there is a finite triplet P gap. A small fraction of the phenomenological repulsion of the original UIX interaction is already sufficient to close the gap. It's unclear whether the introduction of short-range correlations can reverse this behavior [43]. For a review of many-body methods employed to study superfluidity, see Ref. [44].

Based on the available literature, one may conclude that the impact of including 3NFs or other medium effects in calculations of the triplet pairing gap in neutron matter vary wildly, both quantitatively and qualitatively, depending on the specifics of the input. Systematic studies with robust 2NFs and 3NFs are called for. At the same time, availability of more and more accurate data from INS is crucial to constrain all important aspects of the theoretical input.

Acknowledgments

This work was supported by the U.S. Department of Energy, Office of Science, Office of Basic Energy Sciences, under Award Number DE-FG02-03ER41270.

The authors are grateful to Dany Page for help with the NSCool cooling simulation package.

References

1. [△]Abbott BP, et al. *GW170817: Observation of Gravitational Waves from a Binary Neutron Star Inspiral*. *P hys. Rev. Lett.* **119**(16):161101 (2017). doi:[10.1103/PhysRevLett.119.161101](https://doi.org/10.1103/PhysRevLett.119.161101). arXiv:[1710.05832](https://arxiv.org/abs/1710.05832).

2. [^]Abbott BP, et al. Multi-messenger Observations of a Binary Neutron Star Merger. *Astrophys. J. Lett.*. **84** 8(2): L12 (2017). doi:[10.3847/2041-8213/aa91c9](https://doi.org/10.3847/2041-8213/aa91c9). arXiv:[1710.05833](https://arxiv.org/abs/1710.05833).
3. [^]Abbott BP, et al. GW170817: Measurements of neutron star radii and equation of state. *Phys. Rev. Lett.*. **121**(16):161101. doi:[10.1103/PhysRevLett.121.161101](https://doi.org/10.1103/PhysRevLett.121.161101). arXiv:[1805.11581](https://arxiv.org/abs/1805.11581).
4. [^]Abbott BP, et al. (2019). "GWTC-1: A Gravitational-Wave Transient Catalog of Compact Binary Mergers Observed by LIGO and Virgo during the First and Second Observing Runs". *Phys. Rev. X*. **9**: 031040.
5. [^]Miller MC, et al. (2019). "PSR J0030+0451 mass and radius from NICER and implications for the properties of neutron star matter". *Astrophys. J. Lett.*. **887**: L24.
6. ^a ^bMiller MC, et al. (2021). "The Radius of PSR J0740+6620 from NICER and XMM-Newton Data". *Astrophys. J. Lett.*. **918** (2): L28. doi:[10.3847/2041-8213/aco89b](https://doi.org/10.3847/2041-8213/aco89b). arXiv:[2105.06979](https://arxiv.org/abs/2105.06979).
7. ^a ^bHuth S, et al. (2022). "Constraining neutron-star matter with microscopic and macroscopic collisions". *Nature*. **606**: 276.
8. [^]Sammarruca F. The Neutron Skin of ^{48}Ca and ^{208}Pb : A critical analysis. *Symmetry*. **16** (2024): 34. doi:[10.3390/sym16010034](https://doi.org/10.3390/sym16010034).
9. ^a ^b ^cRomani RW, Kandel D, Filippenko AV, Brink TG, Zheng W (2022). "PSR J0952-0607: The Fastest and Heaviest Known Galactic Neutron Star". *Astrophys. J. Lett.*. **934**: L18. arXiv:[2207.05124](https://arxiv.org/abs/2207.05124).
10. [^]Potekhin AY, Zyuzin DA, Yakovlev DG, Beznogov MV, Shibano YA (2020). "Thermal luminosities of cooling neutron stars". *Monthly Notices of the Royal Astronomical Society*. **496**: 5052.
11. ^a ^bSammarruca F, Millerson R (2021). "Analysis of the neutron matter equation of state and the symmetry energy up to fourth order of chiral effective field theory". *Phys. Rev. C*. **104** (3): 034308. doi:[10.1103/PhysRevC.104.034308](https://doi.org/10.1103/PhysRevC.104.034308). arXiv:[2106.11282](https://arxiv.org/abs/2106.11282).
12. [^]Sammarruca F, Millerson R (2021). "Overview of symmetric nuclear matter properties from chiral interactions up to fourth order of the chiral expansion". *Phys. Rev. C*. **104** (6): 064312. doi:[10.1103/PhysRevC.104.064312](https://doi.org/10.1103/PhysRevC.104.064312). arXiv:[2109.01985](https://arxiv.org/abs/2109.01985).
13. [^]Sammarruca F, Millerson R. "The Equation of State of Neutron-Rich Matter at Fourth Order of Chiral Effective Field Theory and the Radius of a Medium-Mass Neutron Star". *Universe*. **8**(2):133. doi:[10.3390/universe8020133](https://doi.org/10.3390/universe8020133). arXiv:[2202.13475](https://arxiv.org/abs/2202.13475).
14. [^]Furnstahl RJ, Klco N, Phillips DR, Wesolowski S (2015). "Quantifying truncation errors in effective field theory". *Phys. Rev. C*. **92** (2): 024005. doi:[10.1103/PhysRevC.92.024005](https://doi.org/10.1103/PhysRevC.92.024005). arXiv:[1506.01343](https://arxiv.org/abs/1506.01343).
15. [^]Machleidt R, Sammarruca F (2024). "Recent advances in chiral EFT based nuclear forces and their applications". *Journal of Progress in Particle and Nuclear Physics*. **137**: 104117.

16. ^{a, b, c}Epelbaum E, Krebs H, Reinert P (2020). "High-precision nuclear forces from chiral EFT: State-of-the-art, challenges and outlook". *Front. in Phys.*. 8: 98. doi:[10.3389/fphy.2020.000098](https://doi.org/10.3389/fphy.2020.000098). arXiv:[1911.11875](https://arxiv.org/abs/1911.11875).
17. [^]Epelbaum E, Krebs H, Reinert P (2022). "Semi-local nuclear forces from chiral EFT: State-of-the-art and challenges." arXiv. [arXiv:2206.07072 \[nucl-th\]](https://arxiv.org/abs/2206.07072).
18. [^]Bernard V, Epelbaum E, Krebs H, Meissner U-G. Subleading contributions to the chiral three-nucleon force. I. Long-range terms. *Phys. Rev. C.* 77 (2008): 064004. doi:[10.1103/PhysRevC.77.064004](https://doi.org/10.1103/PhysRevC.77.064004). arXiv:[0712.1967](https://arxiv.org/abs/0712.1967).
19. [^]Bernard V, Epelbaum E, Krebs H, Meissner UG (2011). "Subleading contributions to the chiral three-nucleon force II: Short-range terms and relativistic corrections". *Phys. Rev. C.* 84: 054001. doi:[10.1103/PhysRevC.84.054001](https://doi.org/10.1103/PhysRevC.84.054001). arXiv:[1108.3816 \[nucl-th\]](https://arxiv.org/abs/1108.3816).
20. ^{a, b}Krebs H, Epelbaum E (2023). "Towards consistent nuclear interactions from chiral Lagrangians I: The path integral approach." arXiv. [arXiv:2311.10893 \[nucl-th\]](https://arxiv.org/abs/2311.10893).
21. [^]Krebs H, Epelbaum E (2023). "Towards consistent nuclear interactions from chiral Lagrangians II: Symmetry preserving regularization." arXiv. [arXiv:2312.13932 \[nucl-th\]](https://arxiv.org/abs/2312.13932).
22. ^{a, b}Entem DR, Machleidt R, Nosyk Y (2017). "High-quality two-nucleon potentials up to fifth order of the chiral expansion". *Phys. Rev. C.* 96 (2): 024004. doi:[10.1103/PhysRevC.96.024004](https://doi.org/10.1103/PhysRevC.96.024004). arXiv:[1703.05454](https://arxiv.org/abs/1703.05454).
23. ^{a, b, c}Sammarruca F, Millerson R (2022). "The Equation of State of Neutron-Rich Matter at Fourth Order of Chiral Effective Field Theory and the Radius of a Medium-Mass Neutron Star". *Universe.* 8: 133.
24. [^]Read JS, Lackey BD, Owen BJ, Friedman JL (2009). "Constraints on a phenomenologically parameterized neutron-star equation of state". *Phys. Rev. D.* 79: 124032. doi:[10.1103/PhysRevD.79.124032](https://doi.org/10.1103/PhysRevD.79.124032). arXiv:[0812.2163 \[astro-ph\]](https://arxiv.org/abs/0812.2163).
25. ^{a, b}Kanakakis-Pegios A, Koliogiannis PS, Moustakidis CC (2021). "Probing the Nuclear Equation of State from the Existence of a $\approx 2.6 M_{\odot}$ Neutron Star: The GW190814 Puzzle". *Symmetry.* 13: 183.
26. ^{a, b}Tews I, Carlson J, Gandolfi S, Reddy S (2018). "Constraining the speed of sound inside neutron stars with chiral effective field theory interactions and observations". *Astrophys. J.* 860 (2): 149. doi:[10.3847/1538-4357/aac267](https://doi.org/10.3847/1538-4357/aac267). arXiv:[1801.01923](https://arxiv.org/abs/1801.01923).
27. [^]Fonseca E, Cromartie HT, Pennucci TT, Ray PS, Kirichenko AY, et al. (2021). "Refined Mass and Geometric Measurements of the High-Mass PSR J0740 + 6620". *Astrophys. J. Lett.* 915: L12.
28. ^{a, b}Kumar M, Kumar S, Thakur V, Kumar R, Agrawal BK, Dhiman SK (2023). "CREX- and PREX-II-motivated relativistic interactions and their implications for the bulk properties of nuclear matter and neutron stars". *Phys. Rev. C.* 107: 055801.

29. ^a ^bSammarruca F. Contribution of isovector mesons to the symmetry energy in a microscopic model. *Phys. Rev. C.* **84** (2011): 044307.
30. [^]Wei JB, Burgio GF, Schulze H-J, Zappala` D (2020). "Cooling of hybrid neutron stars with microscopic equations of state". *Mon. Not. R. Astron. Soc.* **498**: 344.
31. [^]Yakovlev DG, Kaminker AD, Gnedin OY, Haensel P (2001). "Neutrino emission from neutron stars". *Phys. Rept.* **354**: 1. doi:[10.1016/S0370-1573\(00\)00131-9](https://doi.org/10.1016/S0370-1573(00)00131-9). arXiv:[astro-ph/0012122](https://arxiv.org/abs/astro-ph/0012122).
32. [^]Richardson MB, van Horn HM, Ratcliff KF, Malone RC (1982). "Neutron star evolutionary sequences". *ApJ.* **255**: 624R.
33. ^a ^bDas HC, Wei JB, Burgio GF, Schulze HJ (2024). "Neutron star cooling and mass distributions". arXiv. [arXiv:2403.02222v2](https://arxiv.org/abs/2403.02222v2).
34. [^]Gonzalez-Jimenez N, Petrovich C, Reisenegger A (2015). "Rotochemical heating of millisecond and classical pulsars with anisotropic and density-dependent superfluid gap models". *MNRAS.* **447**: 2073.
35. [^]Gonzalez-Caniulef D, Guillot S, Reisenegger A (2019). "Neutron star radius measurement from the ultraviolet and soft X-ray thermal emission of PSR J0437-4715". *MNRAS.* **490**: 5848.
36. [^]Potekhin AY, Zyuzin DA, Yakovlev DG, Beznogov MV, Shibano YA (2020). "Thermal luminosity of cooling neutron stars". *Mon. Not. R. Astron. Soc.* **496**: 5052.
37. ^a ^bPotekhin AY, Chabrier G, Yakovlev DG (1997). "Internal temperatures and cooling of neutron stars with accreted envelopes". *A&A.* **323**: 415.
38. ^a ^bNomoto K, Tsuruta S (1987). "Cooling of neutron stars: Effects of the finite time scale of thermal conduction". *ApJ.* **312**: 711.
39. [^]Krotscheck E, Papaconstantinou P, Wang J (2023). "Variational and parquet-diagram calculations for neutron matter. V. Triplet pairing". arXiv. [arXiv:2308.00873](https://arxiv.org/abs/2308.00873).
40. ^a ^bRios A, Polls A, Dickhoff WH. "Pairing and short-range correlations in nuclear systems". *J. Low Temp. Phys.* **189** (5-6): 234-249. doi:[10.1007/s10909-017-1818-7](https://doi.org/10.1007/s10909-017-1818-7). arXiv:[1707.04140](https://arxiv.org/abs/1707.04140).
41. [^]Zuo W, Cui CX, Lombardo U, Schulze HJ. "Three-body force effect on P-3 F-2 neutron superfluidity in neutron matter, neutron star matter, and neutron stars". *Phys. Rev. C.* **78** (2008): 015805. doi:[10.1103/PhysRevC.78.015805](https://doi.org/10.1103/PhysRevC.78.015805).
42. [^]Drischler C, Krüüoofcger T, Hebeler K, Schwenk A (2017). "Pairing in neutron matter: New uncertainty estimates and three-body forces". *Phys. Rev. C.* **95** (2): 024302. doi:[10.1103/PhysRevC.95.024302](https://doi.org/10.1103/PhysRevC.95.024302). arXiv: [1610.05213](https://arxiv.org/abs/1610.05213).

43. ^{a, b}Papakonstantinou P, Clark JW. "Three-Nucleon Forces and Triplet Pairing in Neutron Matter". *J. Low Temp. Phys.* 189 (5-6): 361–382. doi:[10.1007/s10909-017-1808-9](https://doi.org/10.1007/s10909-017-1808-9). arXiv:[1705.10463](https://arxiv.org/abs/1705.10463).

44. [^]Sedrakian A, Clark JW (2019). "Superfluidity in nuclear systems and neutron stars". *Eur. Phys. J. A.* 55 (9): 167. doi:[10.1140/epja/i2019-12863-6](https://doi.org/10.1140/epja/i2019-12863-6). arXiv:[1802.00017](https://arxiv.org/abs/1802.00017).

Declarations

Funding: This work was supported by the U.S. Department of Energy, Office of Science, Office of Basic Energy Sciences, under Award Number DE-FG02-03ER41270. The authors are grateful to Dany Page for help with the NSCool cooling simulation package.

Potential competing interests: No potential competing interests to declare.